Benjamin Emley
Materials Science and Engineering Program,
University of Houston,
4726 Calhoun Road,
Houston, TX 77204
e-mail: bjemley@uh.edu

Dhruba Panthi
Department of Engineering Technology,
Kent State University at Tuscarawas,
330 University Drive NE,
New Philadelphia, OH 44663
e-mail: dpanthi@kent.edu

Yanhai Du
College of Aeronautics and Engineering,
Kent State University,
1400 Lefton Esplanade,
Kent, OH 44242
e-mail: ydu5@kent.edu

Yan Yao[1]
Materials Science and Engineering Program;
Department of Electrical and Computer
Engineering and Texas Center for
Superconductivity,
University of Houston,
4726 Calhoun Road,
Houston, TX 77204
e-mail: yyao4@uh.edu

Controlling Porosity of Anode Support in Tubular Solid Oxide Fuel Cells by Freeze Casting

Precise porosity control is highly desirable for improving the electrochemical performance of solid oxide fuel cells (SOFCs). Freeze casting is an established method for enabling high bulk porosity in structures and controlling pore orientation. In this study, freeze casting was used to fabricate tubular, anode-supported SOFCs with aligned and varying amounts of porosity by controlling the solids/water ratio in different casting slurries. SOFCs were prepared with a Ni/yttria and scandia stabilized zirconia (ScYSZ) anode support (AS), an anode functional layer (AFL), a ScYSZ electrolyte, a lanthanum strontium manganite (LSM)/ScYSZ cathode interlayer (CIL), and an LSM cathode. The permeability of the anode support was found to increase from 1.4×10^{-2} to 1.8×10^{-2} m^2 as porosity was increased from 57 to 64 vol%, while the total cell resistance decreased by 35% from 0.93 to 0.60 Ohm cm^2. When evaluated with 30 vol% H_2 as the fuel at 800 °C, the decrease of concentration polarization enabled an increase in electrochemical performance by 42% from 0.35 to 0.50 W/cm^2 as the porosity in the anode support was increased. Mechanical strength characterization using a three-point method showed there is a practical upper limit of the amount of porosity that can be designed into the anode support. This work paves a way for controlling porosity by freeze casting and understanding the correlation between porosity and concentration polarization losses in SOFCs.
[DOI: 10.1115/1.4046489]

Keywords: freeze casting, porosity concentration, tubular SOFC, mass transport resistance, Darcy's permeability, advanced materials characterization, electrochemical storage, fuel cells, innovative material synthesis and manufacturing methods

1 Introduction

A solid oxide fuel cell (SOFC) is an electrochemical device that generates electricity directly from the chemical energy stored in fuels and with high-energy conversion efficiency [1,2]. A SOFC can operate with a variety of fuels including industrial grade hydrogen, natural gas, propane, and diesel and can operate nearly silently as an open, energy conversion system [3,4]. Compared with planar configurations, tubular SOFCs require less or no sealing and have shown high endurance against thermal cycling allowing for fast start-up and shut-down operations [5–8].

Lowering the tortuosity of fuels diffusing through the porous anode [9–11] has become a hot topic over the past decade, because the anode is often the thickest layer of a SOFC [12,13]. Gaseous diffusion through the anode support (AS) may be improved by enhancing anode porosity using pyrolyzable pore formers such as starch, carbon black, graphite, cellulose, and polymer beads [14–18]. Haslam et al. studied the effect of anode porosity and reported that the best performance was achieved at 61 vol% porosity [14]. Suzuki et al. demonstrated a significant improvement in the power performance by developing a porous anode microstructure using polymethyl methacrylate (PMMA) beads as a pore forming agent in the bulk anode support [18]. The sample with the highest porosity of 57 vol% demonstrated the highest power density.

Phase inversion and freeze casting are two methods recognized for making the support structure of a SOFC with aligned porosity. Phase inversion method utilizes toxic organic solvents such as N-methyl-2-pyrrolidone, which raises concerns about hazards to the environment for forming the support [19]. Freeze casting can utilize water as the processing solvent to make the supporting structure, which is environmentally friendly. Chen et al. were the first to apply the dual tape/freeze casting method to develop an anode-supported planar SOFC, and they demonstrated a maximum power density of 1.28 W/cm^2 at 800 °C [20]. In their work, the total polarization resistance was 0.16 Ω cm^2 while operating with hydrogen fuel and having 42 vol% porosity in the freeze-casted anode. A few other groups have reported the application of freeze casting to produce SOFC components including anode and cathode supports [21–25]. Moon et al. fabricated tubular anode supports by freeze casting and with controllable porosity from 35 to 60 vol% in a sintered anode substrate [26]; however, they did not report electrochemical performance. Some of us compared the microstructure of tubular anode supports fabricated by three freeze casting techniques, referred as gel-casting, center pin method, and freeze and drain method and identified the freeze and drain method is the most promising to fabricate tubular SOFCs [27]. Recently, we further improved the freeze and drain method and electrochemically evaluated a tubular SOFC made of Ni/YSZ-YSZ-LSM/YSZ-LSM, showing the maximum power density of 0.47 W cm^2 at 800 °C with 50 vol% of hydrogen [28]. The porosity of the anode support was 64 vol%.

In this work, we varied the porosity of tubular anode supports utilizing the freeze casting method with the goal to better understand the correlation between porosity and concentration polarization losses in SOFCs. The porosity was controlled by varying the solids/water weight ratio when preparing anode slurries with all other processing conditions kept constant. Additionally, the permeability and mechanical strength were characterized as a function of porosity.

[1]Corresponding author.

Manuscript received October 24, 2019; final manuscript received February 20, 2020; published online February 28, 2020. Assoc. Editor: Kevin Huang.

2 Experimental Details

2.1 Preparation of Slurries for Freeze Casting. The anode slurry was prepared by mixing NiO (Type F, Novamet, Lebanon, TN) and 10Sc1YSZ (Daiichi Kigenso, Japan) powders in a 3:2 weight ratio into 19.5–42.0 wt% deionized water containing 0.7–1.0 wt% Darvan® C-N (Vanderbilt Minerals, LLC, Gouverneur, NY) used as a dispersing agent. Next, 5.5–7.6 wt% Duramax™ B-1000 and 5.5–7.6 wt% Duramax™ B-1022 (DOW, Midland, MI) polyacrylic latex resins were added followed by 0.6–0.9 wt% of Foamstar® ST 2412 (BASF, Florham Park, NJ) as a surface tension modifier and defoamer. The ratio between the two Duramax™ polymer resins was kept constant at 1:1 in each of three anode formulations prepared. The three formulations used were based primarily upon changing the total amount of water added to each slurry and are later identified as *W*1, *W*2, and *W*3 representing slurries having 19.5, 29.1, and 42.0 wt% deionized water and 63.5, 55.9, and 45.7 wt% ceramic powders, respectively. Table S1 available in the Supplemental Materials on the ASME Digital Collection shows the materials by wt% and in order of addition to prepare each of the three anode slurries used for freeze casting. Each slurry, less the mixing beads, was stirred inside of a glass beaker with a magnetic stir bar for 15 min prior to casting and then strained through a disposable, 190-μm mesh to extract any abnormal polymeric agglomerates immediately prior to the freeze casting process.

2.2 Freeze Casting Anode Supports. The method for freeze casting the ceramic tubes in this study followed the freeze and drain method described in previous work [27] and is briefly discussed here. The casting mold was chilled with working fluid (Dowtherm SR-1, DOW, Midland, MI) circulated at maximum speed by a programmable, recirculating chiller (Vivtek VIV-DC40-06, China). Formation of an ice barrier layer (IBL) was done after programming the chiller to −5.0 °C while freeze casting of the anode supports was done when the chiller was programmed to −15.0 °C. The rate of filling the casting channels with either water to form the IBL or anode slurry to form the anode support was constant at ∼30 cm^3/min. The dwelling periods for each slurry while forming the anode support during freeze casting were 7, 15, and 20 s, respectively, for samples identified as *W*1, *W*2, and *W*3. After the dwelling period, the excess slurry was quickly drained from the casting channel by suction at the bottom and then the circulating chiller was programmed to −5 °C.

2.3 Freeze Drying Anode Support Tubes. A rubber stopper hermetically sealed the bottom of each casting channel, while a single bore rubber stopper was inserted at the top of the casting channel. Gas-tight tubing connected the single bore rubber stopper at the top of the casting channel to a port on a freeze-drying system (Columbia International, Columbia, SC). The vacuum pressure of casting channels was then reduced with a VZX-120L rotary vane vacuum pump (Columbia International, Columbia, SC) connected to the freeze-drying system and having a rated air displacement of 120 l/min. The absolute pressure of the system was measured by the freeze dryer and reached between 10 and 20 Pa and was held constant during the freeze-drying period. The mold temperature was maintained at a subzero temperature of −4.5 °C by programming the recirculating chiller to operate for 3 hours after which the chiller was shut-off, and the temperature of the mold was permitted to convectively increase to room temperature while the tubes remained under vacuum. The freeze-drying period at room temperature continued overnight or ∼12 h. When all of the ice inside of the casting channels was sublimed and transferred to the freeze dryer, the five dried tubes were carefully removed and pre-sintered vertically by way of a alumina pin and supporting plate (99.9% aluminum oxide) in air at 1100 °C for 2 h inside of a standard muffle furnace.

2.4 Coating Functional Layers. To make the full SOFC, four slurries were prepared for dip coating the anode functional layer (AFL), the electrolyte, the cathode interlayer (CIL), and the cathode. The thickness of the AFL was increased by using three sequential coatings of the AFL slurry separated by 10 min of drying in air. The electrolyte, CIL, and cathode slurries were dip-coated just one time each. The dunk speed, dwell time, and removal speed were 1 mm/s, 8 s, and 1 mm/s, respectively, for all dip coatings.

The AFL slurry contained NiO (Type F, Novamet, Lebanon, TN) and 10Sc1YSZ (Daiichi Kigenso, Japan) powders in a 1:1 weight ratio mixed in a binary solvent system of 2-butanone and ethanol, both being >95% pure (1:1 by weight). The ceramic solid concentration of the AFL with respect to the total slurry weight was 41%, and each of the following additions was based upon the total weight of the slurry. Polyvinyl butyral (PVB; B-76, Eastman, Kingsport, TN) at 2.2 wt% was added as a binder. Polyvinyl pyrrolidone with an average MW of 10,000 (PVP-10; Sigma Aldrich, St. Louis, MO) at 1.1 wt% was added as a dispersant. Dioctyl phthalate (DOP; Sigma Aldrich, St. Louis, MO) at 1.5 wt% was added as a plasticizer. And, polyethylene glycol with a MW of 400 (PEG-400, Sigma Aldrich, St. Louis, MO) at 1.5 wt% was added as a homogenizer. Prior to dip coating, the slurry was milled and homogenized for 30 min using a high-energy vibratory ball mill (Col-Int Tech, Irmo, SC). A 60 mL HDPE Nalgene bottle with 50 g of round, stabilized zirconia beads (ϕ:6 mm, Inframat Materials, Manchester, CT) was used during the milling of the slurry. After all dip coatings, the AFL coatings were dried in air for an additional 2 hours before pre-sintering the anode support and AFL coatings at 1100 °C.

The same solvents and organic additives were used to prepare the electrolyte, CIL, and cathode dipping slurries, as well as the same milling method to homogenize the slurry contents prior to dip coating. The electrolyte slurry was made by dispersing 33 wt% 10Sc1YSZ (Daiichi Kigenso, Japan) in the 2-butanone–ethanol solvent along with 2.2 wt% of binder, dispersant, and plasticizer, each. After dip coating the ScYSZ electrolyte slurry on top of the anode functional layer, the support and coatings were co-sintered in air at 1480 °C for 2 h.

The CIL was made with an A-site deficient strontium-doped lanthanum manganite (LSM; $(La_{0.8}Sr_{0.2})_{0.97}MnO_3$, Praxair, Woodinville, WA) and 10Sc1YSZ (Daiichi Kigenso, Japan) in a 1:1 weight ratio, whereas the cathode layer contained only LSM. The solids concentrations of the CIL and cathode slurries were both 40 wt% and consisted of 2.2 wt% of binder, dispersant, and plasticizer, each, with respect to the total slurry weight. Parafilm was used to mask the ends of the support prior to the cathode coatings but specifically exposed an area resulting with a total cathode active area of ∼1 cm^2 with a ∼3 mm gap between the end of the cathode and the anode current collection at one end of the support. The CIL and cathode layers were dip-coated successively onto the co-sintered half-cells with approximately 30 min of drying time in air after the CIL coating. The coatings were dried together in air for two additional hours before the parafilm masks were carefully removed and before the CIL and the cathode layers were co-sintered in air at 1150 °C for 2 h.

The 12 steps for fabricating the tubular SOFC starting with the preparation of slurries for freeze casting the anode support are summarized in Fig. 1(*a*). The heating ramp to and from the target temperatures for all pre-sintering and sintering cycles was 2.5 °C/min. All sintering was done in a standard muffle furnace with MoS_2 heating elements. During sintering, the tubes were arranged vertically to avoid any physical contact between the fuel cell functional components and insulative components of the furnace, typically alumina silicate fibers [29].

2.5 Preparation of Tubes for Evaluations. Three types of tubes were prepared for the different evaluations in this study. The first is the bare, freeze-casted anode support tube which did not receive any additional coatings before it was sintered in air at

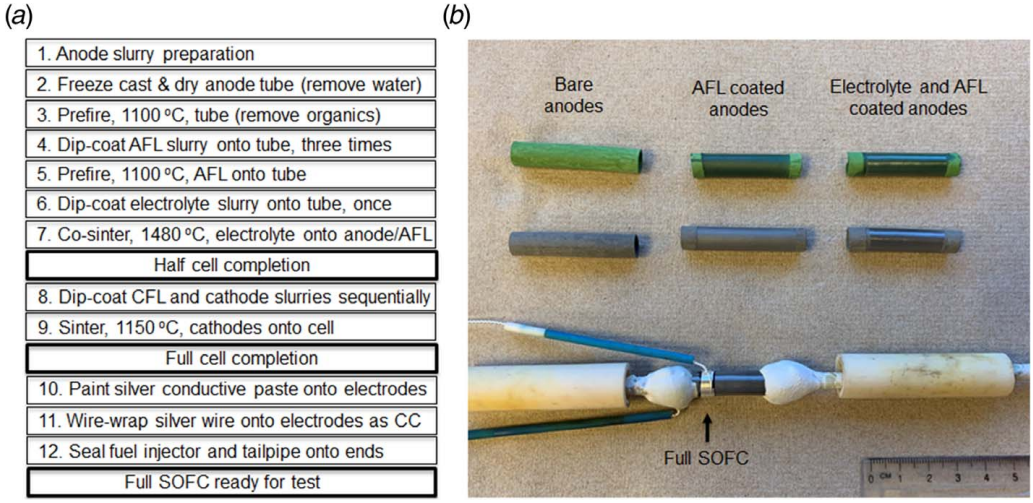

Fig. 1 (*a*) Procedure for preparing complete, tubular SOFCs having the composition of LSM(C)/LSM-ScYSZ(CIL)/ScYSZ(*E*)/NiO-ScYSZ(AFL)/NiO-ScYSZ(AS) starting from a freeze-casted AS. Within the procedure for wire-wrapping, "CC" is an abbreviation for current collectors. (*b*) Tubes taken from three stages of the processing schematic and then sintered to 1480 °C in air for 2 hours. The top row of tubes is when the tubes are in their natural oxidized state with NiO in their structures while bottom row of tubes show them in their reduced state with Ni. The assembly at the bottom represents a full SOFC ready for electrochemical evaluation.

1480 °C for 2 h. The second is a freeze-casted anode support tube that is pre-sintered in air at 1100 °C for 2 hours prior to being coated with the AFL, and then sintered in air at 1480 °C for 2 h. The third follows the procedure above to prepare a full testable SOFC.

After sintering, the first two types of tubes described above were reduced in hydrogen at 800 °C. The tubes were individually placed inside the middle of a 1 in. diameter quartz tube that is then placed inside of a tube furnace with a 6 in. hot zone, so that the prepared tubes were approximately in the middle of the furnace's hot zone. The ends of the quartz tube extended outside of the hot zone where a secure gas connection was made at the inlet for hydrogen while the other end is left open-ended to atmosphere as the outlet. Pictures of tubes after selected processing stages and after sintering to 1480 °C for 2 hours as well as a full cell ready for electrochemical evaluations are shown in Fig. 1(*b*).

2.6 Permeability Evaluation. Gas permeability of sintered freeze-casted anode supports with and without AFL coatings were measured using a custom device. Before each evaluation, one end of an anode support was connected to a source of methane gas regulated to different flowrates by a mass flow controller. The pressure of the methane gas flowing through the anode support changed depending upon the programmed flowrate and was monitored with a pressure gauge, *P*1, having a range from 0 to 7.500 kPa above atmosphere. The other end of the anode support was capped and sealed so that the flow of methane gas was forced to permeate through the anode support to the collection side. The anode support with its gas connection was inserted into a larger quartz tube such that the gas pressure of the atmosphere surrounding the outside of the anode support, designated as the collection side, could be monitored with a second pressure gauge, *P*2. A sweep gas of N_2 flowing over the outside of the anode support on the collection side was controlled at 50 ml/min by another mass flow controller. After each measurement was taken, the flow of methane was incrementally increased which consequently changed the pressure between *P*1 and *P*2 and was recorded as ΔP.

2.7 Microstructure Evaluation. After electrochemical evaluations, the microstructure of the carbon coated SOFC samples was examined using a Gemini LEO (Zeiss) field emission scanning electron microscope (SEM, White Plains, NY). The open porosity of the freeze cast anode supports was measured by Archimedes' method using deionized water as the displacement liquid.

2.8 Electrochemical Evaluation. The electrochemical performance of the tubular SOFCs was evaluated with a potentiostat (PGSTAT302N, Metrohm Autolab, Netherlands) equipped with a frequency response analyzer. For cathode current collection, conductive silver paste (Sigma Aldrich, St. Louis, MO) was hand painted onto the surface of the cathode with careful attention not to allow any silver paint to contact the electrolyte coating adjacent to the ends of the cathode. For anode current collection, the same conductive silver paste was hand painted over an exposed surface of the anode at one of the ends, closest to the cathode active area. The silver conductive paste was dried in air at 125 °C for 2 hours. Current collection wires made of fine silver (Ø 0.5 mm; Hoover and Strong, N. Chesterfield, VA) were tightly wound around the dried silver conductive paste on the cathode and anode. The injector and exhaust pipe were sealed to a SOFC by using a two-part alumina sealant and adhesive cement (Aluseal; Sauereisen, Pittsburgh, PA). The assembly of test-ready SOFC is shown at the bottom of Fig. 1(*b*).

SOFCs were heated at 5 °C/min to a soaking temperature of 800 °C, and when the furnace reached 800 °C, a mixture of H_2 and N_2 (30 vol% H_2) was delivered to the anode via the injector. The fuel consisting of H_2 and N_2 was maintained at 200 ml/min and was measured with an inline pressure gauge connected to the fuel line at 250 Pa above atmosphere, for all SOFCs evaluated. Air was sent around the cathode at 600 ml/min and considered in excess. The concentration of H_2 to the anode was varied in a range from 10 to 30 vol% during a series of electrochemical evaluations on the three different SOFCs prepared. The impedance measurements were conducted under open circuit voltage (OCV) conditions by applying an AC perturbation of 50 mV over a frequency range from 100 kHz to 100 mHz at different temperatures and with different concentrations of H_2 in the anode fuel.

2.9 Mechanical Strength Evaluation. The flexural strength of the sintered freeze-casted anode supports with and without AFL coatings was determined by a three point setup within a

universal tester (Instron) having a maximum load capacity of 2 kN. A displacement rate of 1 mm/s was used to apply the load and the resulting response expressed as the modulus of rupture (MOR) reported in units of MPa.

3 Results and Discussion

Freeze casting was done with an aluminum mold shaped as a rectangular prism having five cylindrical casting channels as shown in Fig. S1(*a*) available in the Supplemental Materials on the ASME Digital Collection. The five casting channels with a diameter of 12.5 mm are separated between six chilling channels. The surfaces of the casting channels are smooth while the chilling channels are threaded for 3/8 in. NPT pipe connections at each end. Single bore rubber stoppers with tubing connections were used at the ends of casting channels to allow injections of water and ceramic slurry via a syringe and with a fill-direction of the casting channel from bottom to top. The sides of the mold were covered with insulative plastic foam during freeze casting to help reduce heat transfer between the chilled mold and the ambient temperature. The packaged mold is shown in Fig. S1(*b*) available in the Supplemental Materials on the ASME Digital Collection.

The IBL was applied to enable removal of the tube from the mold [28] after freeze drying. The dwelling period, defined as the amount of time the casting channel was filled with ceramic slurry during which ice crystals were growing, was modified so that each tube would have approximately the same thickness. Prior development demonstrated that casting slurries with a higher water to ceramic powder ratio required a longer dwelling period to achieve the same wall thickness as a slurry with a lower water to ceramic powder ratio. The slurry with the lowest water to ceramic powder ratio, *W*1, only required ~7 s for a dwelling period inside of the casting channel at −12.5 °C to achieve a tube having about the same wall thickness as the slurry with the highest water to ceramic powder ratio, *W*3, which required 20 s.

The shape of the casting mold used in this study was different compared with earlier work to accommodate five casting channels rather than just one [27,28]. Although this did not change the science of the freeze casting process, the relative convective heat loss from the mold in this study was likely to be larger due to having a lower ratio of the chilling surface area to casting channel surface area. The lower ratio caused a larger differential between the programmed temperature set by the recirculating chiller and the actual temperature of the mold, measured by an independent Type-K thermocouple. The chiller setpoint was programmed to −15 °C during the freeze casting in this study, while the temperature of the mold varied at a higher temperature within a range of −12.3 to −12.7 °C due to heat transfer between the mold and the ambient air. This was a slightly warmer temperature than used in the previous studies [27,28]. Similarly, the temperature of the mold while forming the IBL was −4.5 °C when the chiller was programmed to −5.0 °C.

The polymer binders added to the anode slurry were based upon an acrylic latex that have been used in other freeze casting studies [30,31]. The acrylic latex binders allow for greater flexibility during freeze-drying stage. The tubes were not adversely affected by extending the drying time longer than a minimum time required to sublime the water. Therefore, the drying time was not considered a critical parameter as discussed elsewhere [28]. Initial work in this study showed that the minimum amount time necessary for subliming the water was approximately 5 hours for five casting channels connected in-parallel to the manifold of the freeze dryer. Optimizing the drying time in this study was found to be largely dependent upon reducing the absolute pressure to <10 Pa during freeze drying and then increasing the temperature of the mold to above room temperature after three hours of drying. No differences were observed in dried tubes that were dried with an optimized drying cycle or for an extended drying time. The most important quality was ensuring that all the ice was sublimed and removed from the tube before the tube was removed from the casting channel.

The tubes were cut in half after the first pre-sintering cycle at 1100 °C to increase the number of samples for the different evaluations. The total length of a SOFC anode was ~5 cm, while the average outer diameter was 8.0 ± 0.2 mm after sintering. The target wall thickness of each tube was 650 μm which was controlled by the dwelling times during the freeze casting. The thicknesses of the anode walls representing *W*1, *W*2, and *W*3 were found to be 593, 641, and 635 μm, respectively.

The average volumetric porosities of the anode supports, determined by Archimedes' method, were found to be 57.0%, 61.4%, and 64.0% representing SOFCs identified as *W*1, *W*2, and *W*3, respectively, demonstrating a 7 vol% range of porosity. The data and standard deviation from the measured averages are represented in Fig. 2(*b*). Although the magnitude of porosity matches well with other works that focused on freeze casting [20–22,24–28,30–34], the relatively small range of vol% porosity observed in this study is not reflective of the relatively large differences in the amount of water in each casting slurry. For the different slurries processed, the water to ceramic powder wt. ratio is 0.31, 0.52, and 0.92 for *W*1, *W*2, and *W*3, respectively. This result suggests that extending the range of porosity in the anode supports would require additional processing changes beyond the method described in this study of changing the water to ceramic powder ratio of the casting slurry. Other processing changes that can be incorporated into a freeze casting method to increase the total porosity are suggested elsewhere [28].

Figures 3(*a*)–3(*c*), representing *W*1, *W*2, and *W*3, respectively, show SEM of the fractured cross section of the different anodes prepared for this study. Higher magnification of the cermet lamellas and porosity in each anode support is shown in Figs. 3(*d*)–3(*f*) representing *W*1, *W*2, and *W*3, respectively. The different amount of porosity in the anode supports is difficult to visualize due to the various angles that the lamellas are orientated about the outside, radial boundary. Nonetheless, the plate-like lamellas are shown to be orientated at least in the radial direction to allow for low tortuosity gas transport from the inside to the outside of the tubular structure. The orientation is more apparent for anode supports prepared with less water and having less total porosity, but the size of the pores between the plate-like lamellas is random.

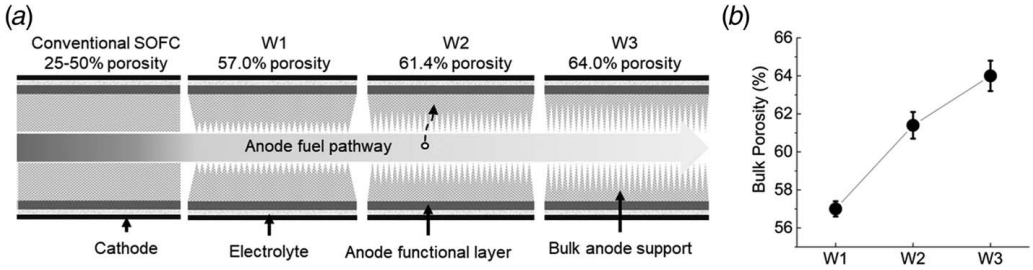

Fig. 2 (*a*) Schematic highlighting the purpose of the study and (*b*) the average porosities of the different anode supports obtained, measured by Archimedes method

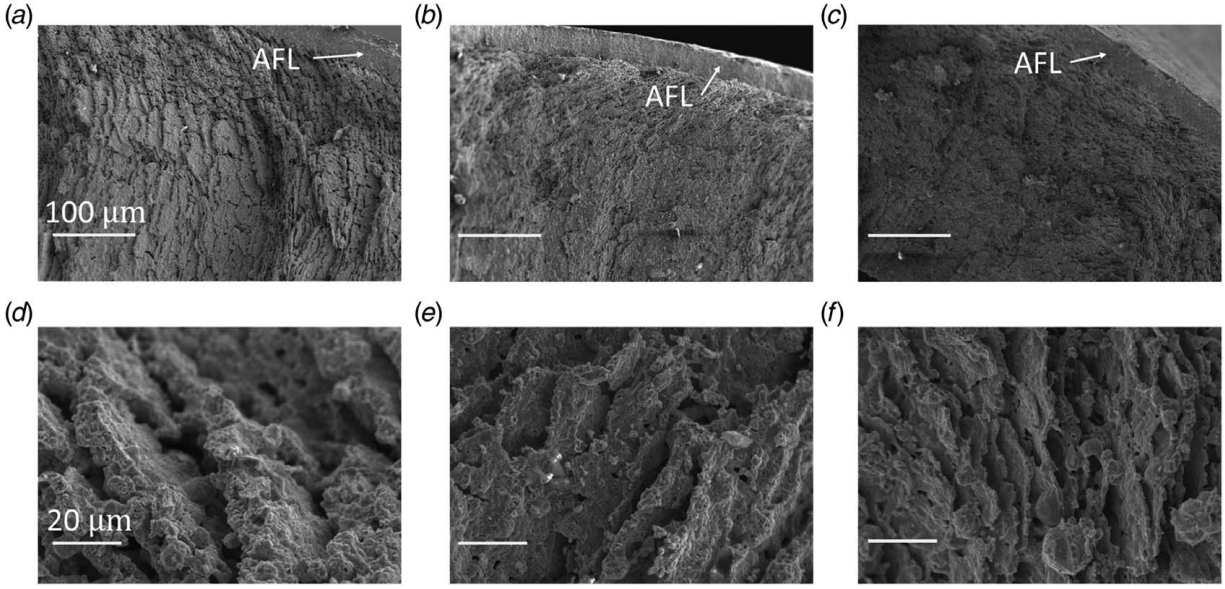

Fig. 3 (*a*–c) SEM images of different anode supports with the outside AFL for samples *W*1, *W*2, and *W*3, respectively. Scale bar: 100 μm. (*d*–*f*) zoom-in SEM images for samples *W*1, *W*2, and *W*3, respectively. Scale bar: 20 μm. All samples composed of an anode and an AFL were sintered and processed to reduce the NiO to Ni.

It is important to note that pore alignment is radial and perpendicular to the surface of the casting channel but is not controlled by any other force to orientate in any additional direction or form of alignment. Particle aggregation that forms between the ice crystals during freeze casting can freely form in any direction 360 deg about this axis, perpendicular to the surface of the casting channel. In other words, the growth of the aggregate and ice moving away from the casting surface is somewhat random. Nonetheless, having pore alignment in one direction, parallel to the radial direction, provides pore channels connecting the inner channel to the outside surface of the anode support which is the most important direction for improving diffusion of fuels through the anode.

Figures 4(*a*)–4(*f*) show the cross-sectional SEM of fractured full cells after electrochemical evaluations. The surface of the freeze-casted anode support in this study has large pores extending from the inside to the outside surfaces of the tube. The open pores on the outside of the tube's surface do not allow for a relatively thin, dense, and leak-tight electrolyte coating to be directly applied to the outer surface of the freeze-casted anode support. Therefore, an AFL was applied to the surface of the anode support primarily as a filler to cover the large pores. The AFL in this study is thicker than what has been used in previous works utilizing freeze casting and specifically those that focus on optimizing the electrochemical performance of a SOFC by addition of an AFL [12,28,35–37]. Without further optimization, the thicker AFL for this study was ~60 μm and was necessary so that its surface was suitable for achieving a dense, non-leaking electrolyte. Future studies should investigate alternative methods to reduce the thickness of the AFL on freeze-casted tubular substrates having maximized porosity. A magnified view between the AFL and the electrolyte is shown in Figs. 4(*d*)–4(*f*) and demonstrates that the outer surface of the AFL is suitable for coating an electrolyte that becomes dense and leak tight. As can be seen, the ScYSZ electrolyte layer is fully dense with only minor closed porosity within the layer and demonstrates good bonding to both Ni-ScYSZ and LSM-ScYSZ functional layers. The thicknesses of the AFL, electrolyte, and cathode were ca. 60, 20, and 30 μm, respectively.

The permeability, k_D (m^2), of a porous anode through which gas permeates can be expressed in Eq. (1) by Darcy's law [38]

$$k_D = \frac{Q\mu d}{A(\Delta P)} \tag{1}$$

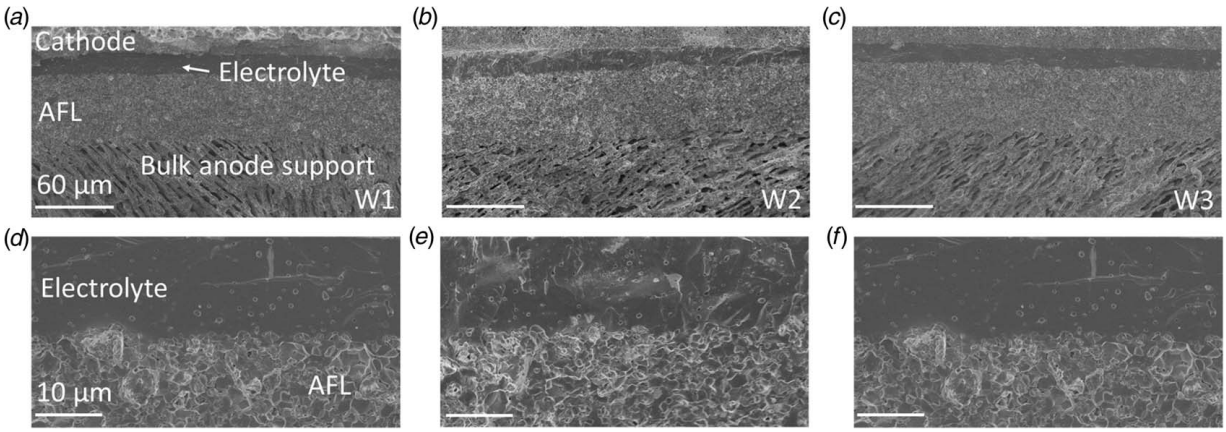

Fig. 4 SEM images showing a fractured cross section of three tested single cells with varying porosity in the freeze-casted anode support. (*a*–c) Scale bar: 60 μm, (*d*–*f*) scale bar: 10 μm. (*a*, *d*) Microstructure of different functional layers in the support, *W*1, 57.0 vol% porosity; (*b*, *e*) *W*2, 61.4 vol% porosity; (*c*, *f*) *W*3, 64.0 vol% porosity; AFL: anode functional layer.

where ΔP (Pa) is the pressure drop along the flow direction through the pores with a thickness, d (m). The flux of gas permeating through the pores is the volumetric flowrate, Q (m^3/s). The absolute viscosity, μ (Pa·s), is specific to the gas used during the evaluation while the area, A (m^2), is the area of the anode tube's walls allowing the gas to permeate from one side to the other.

During this evaluation, H_2 was originally selected as the working gas as it is commonly used for electrochemical evaluations, as done in this study. For any permeation experiment, mass balance at the entry and exit of the test setup is important as any leak in the system invalidates the observation for ΔP. The system setup represented in Fig. 5(*a*) utilized tightly fitted silicone connections to the anode supports in order to connect the working gas to the inlet and outlet. Although the silicone was reasonably tight and while preventing damage to the anode tubes, it was not suitable to maintain 100% mass balance between the inlets and outlets when H_2 was used. As much as 8 vol% of H_2 was lost despite not observing any apparent leaks. Therefore, methane gas was selected to represent a lightweight working gas to substitute the use of H_2. Mass balance analysis showed that 100% of the methane as the working gas was accounted for at the inlet and outlet during permeation evaluations.

Additionally, methane gas is considered appropriate for SOFC technology as some designs include the strategy to directly utilize methane as the anode fuel. Others have reported similar issues using H_2 and consequently have focused on the diffusion properties of methane, carbon dioxide, and carbon monoxide [39].

The flow of methane was controlled by a mass flow controller at room temperature while the absolute viscosity of 1.13×10^{-5} Pa·s was used for calculating the permeability. The permeability of fuel gasses moving through the anode was calculated from observations made using a custom-made setup shown in Fig. 5(*a*). For determining the permeability of the freeze-casted anode supports without AFL coatings, the flow range of 50 ml/min to 400 ml/min of methane was used while a range of 10 ml/min to 80 ml/min was used for anode supports with AFL coatings. The different ranges of flow were necessary to accommodate the limited range of the pressure gauges and what later revealed to be a significant difference in the permeability of anode supports with and without AFL coatings. During each evaluation and as the set flowrate was incrementally increased, the pressure, observed at $P1$, increased as necessary to maintain the set flowrate. The system had an internal pressure drop of ~125 Pa at the highest flowrate of methane moving through the system without any sample (open flow). The pressure at $P2$ was manually adjusted with a needle valve to be 500 Pa above atmosphere to maintain a margin greater than the internal pressure drop of the system. The observed pressure drop across the porous electrode decreases with respect to an increase of its permeability, which varies depending upon its porosity.

Figure 5(*b*) shows the slope of volumetric flowrate through the anode supports with respect to ΔP increases as the volumetric porosity is increased. The permeability, k_D, of anode supports without the AFL is 1.4×10^{-2}, 1.6×10^{-2}, and 1.8×10^{-2} m^2 for anode supports $W1$, $W2$, and $W3$, respectively. Figure 4(*c*) shows the slope of volumetric flowrate through the different anode supports with the same AFL with respect to ΔP also increases as the volumetric porosity is increased. The permeability of anode supports with the AFL is 1.6×10^{-5}, 2.1×10^{-5}, and 2.2×10^{-5} m^2 for anodes identified as $W1$, $W2$ and $W3$, respectively. Figure 4(*d*) shows the permeability of anode supports with and without AFL coatings with respect to anode porosity. These results reveal that the permeability of the anode support with the AFL is three orders of magnitude smaller than that of the anode without AFL despite that the AFL thickness is 10% of the total anode thickness. This observation questions the relevance of slight changes in the porosity of the anode support if the permeation resistance of fuels moving through the anode is largely dominated by that of the AFL, a parameter not varied in this study. Nonetheless, a logical trend is observed with and without AFL coatings that shows an increase in permeability as a function of anode

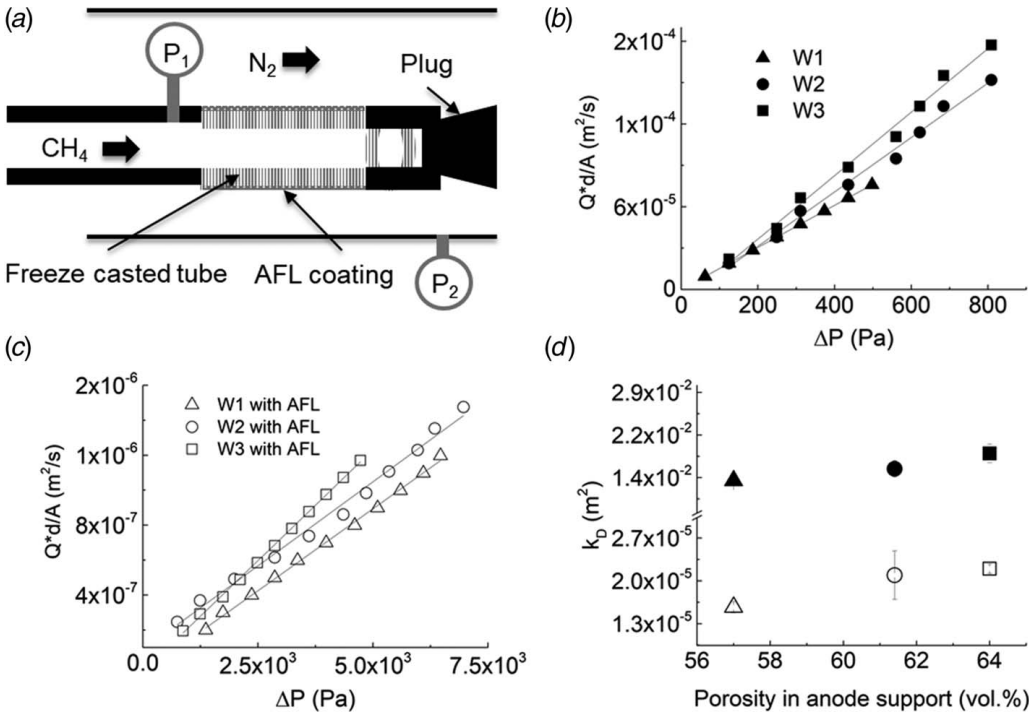

Fig. 5 (*a*) Schematic of the permeation testing setup with an anode support with an AFL coating; (*b*) controlled flux of methane gas, Q^*d/A, of anode supports without AFL coatings and as a function of the pressure drop, ΔP; (*c*) controlled flux of methane gas, Q^*d/A, of anode supports with AFL coatings and as a function of the pressure drop, ΔP; and (*d*) the calculated permeabilities of the anode supports with the AFL (hollow shapes) and without the AFL (filled shapes) coatings with respect to vol% porosity in the anode supports

porosity. This result also suggests future research should focus on methods to reduce the thickness of the AFL.

The impedance of SOFCs with varying porosity in the anode support was evaluated using Nyquist plots under OCV conditions at 800 °C and with different H_2 concentrations in the anode fuel. The different concentrations of H_2 in the anode fuel were used to analyze the different mechanisms that cause change in the concentration polarization of the SOFC. Spectra shown in Fig. 6(*a*) represent SOFCs evaluated with 30 vol% H_2 in the anode fuel while the spectra in Fig. 6(*b*) are those evaluated with 10 vol% H_2 (balance N_2). Both sets of spectra show similar trends with respect to the overall resistance of a SOFC as a function of porosity. Although the total resistance goes down with increasing porosity, the ohmic resistance, as determined by the first intercept at high frequency, goes up, as highlighted with the incepts in Figs. 6(*a*) and 6(*b*).

The impedance was fitted to a Randles equivalent circuit model shown in Fig. 6(*c*) to derive the contributions observed in the impedance. Although there was inductance observed in the results and used in the circuit model, it is ignored in this discussion due to its irrelevance with the study. The contributions to the total resistance, R_T, as determined from the fitted spectra, for the impedance evaluations using 10 to 30 vol% H_2 in the anode fuel at 800 °C as well as the cells evaluated with 30 vol% H_2 at other temperatures are shown in Table S2 available in the Supplemental Materials on the ASME Digital Collection. The impedance spectra for these evaluations are shown in Figs. S2–S4 available in the Supplemental Materials on the ASME Digital Collection.

R_S, the first intercept at high frequency, depends on ohmic losses in the electrolyte, electrodes, and current collecting elements, and thus it is one of the factors to be considered while optimizing the anode porosity. When the H_2 concentration in the fuel was at 30 vol%, a 60% increase in the ohmic resistance is observed, from 0.16 Ohm cm^2 to 0.25 Ohm cm^2 as the anode porosity increases from 57.0 vol% to 64.0 vol%, *W*1 to *W*3. Similarly, a 50% increase in ohmic resistance is observed when the H_2 concentration in the fuel is reduced to 10 vol%. The change in ohmic resistance as a function of anode porosity was not expected. The AFL layer, which is the same for each sample, is relatively thick in this study and could easily carry the current across the relatively short cell length to the current collectors. Nonetheless, future studies could investigate this phenomenon by changing the composition of the anode in order to directly affect its electrical conductivity and to correlate this with relative amounts of porosity.

The first arc observed in each impedance curve which is typically associated with charge transport polarization, R_{CT}. R_{CT} varies as a function of the different porosities in the anode support as shown in Fig. 6(*d*) and shows a maximum for the sample *W*2 having medium porosity. The inflection here is not considered significant as the contribution of R_{CT} for each cell is at least an order of magnitude less than the total resistance and could otherwise be within the noise of the analysis. Additionally, the varying porosity within the anode supports would theoretically have negligible effects on R_{CT} for cells having such relatively thick AFL layers.

The next two arcs moving into the lower frequency regime represent concentration polarizations [18,40–42] and are referred to as R_{Conc1} and R_{Conc2} in the equivalent circuit model. The contributions from these two circuit elements dominate the trend seen in the R_T for each cell measured and under different testing conditions. R_T, which

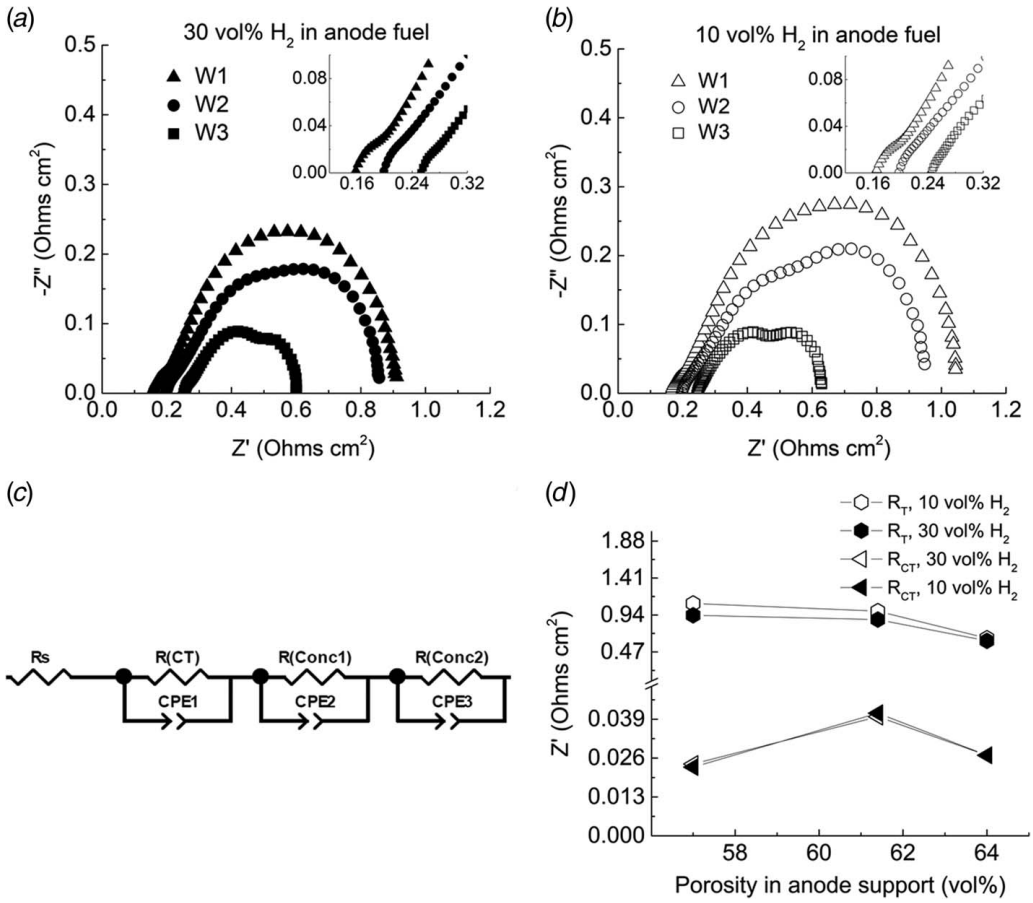

Fig. 6 (*a*) Impedance spectra represented as Nyquist plots of SOFCs with different porosity in the anode support with 30 vol% H_2 in the anode fuel and (*b*) with 10 vol% H_2 in the anode fuel. (c) The Randles circuit used to fit the spectra and (*d*) charge transfer resistance (R_{CT}) and total resistance (R_T) of SOFCs as a function of porosity in the anode support measured at 800 °C and with different concentrations of H_2 in the anode fuel, as indicated.

includes all polarization and ohmic losses, is shown in Fig. 6(*d*) for two different H_2 fuel concentrations and as a function of porosity in the anode support. R_T values were determined by fitting and were 0.93, 0.87, and 0.60 Ohm cm^2 for *W*1, *W*2, and *W*3 cells, respectively, at 800 °C and with 30 vol% H_2 in the anode fuel. When the H_2 in the anode was decreased to 10 vol%, the respective R_T values increased to 1.08, 0.97, and 0.63 Ohm cm^2. Overall, it is apparent that the overall resistance of the different SOFCs went up as H_2 concentration was decreased from 30 to 10 vol% and as porosity within the anode support is decreased. The R_T reduced by 35% by increasing the porosity of the anode support from 57.0 to 64.0 vol% when the anode fuel was 30 vol% H_2. Similarly, R_T is reduced by 42% when the anode fuel is 10 vol% H_2.

I–V polarization curves of single cells at 800 °C with 30 vol% H_2 in the anode fuel are shown in Fig. 7(*a*). As represented in Fig. 7(*b*), the cells showed a maximum power density during their first evaluation of 0.50, 0.45, and 0.35 W/cm^2 with 64.0, 61.4, and 57.0 vol% porosity in the anode support, respectively. A second evaluation was performed after a thermal cycle of each cell and the maximum power densities obtained were 0.52, 0.41, and 0.32 W/cm^2 for SOFCs with 64.0, 61.4, and 57.0 vol% porosity in the anode support, respectively. The performance of the cell with the highest porosity in the anode support goes up slightly while the performances of the other SOFCs decrease slightly. Overall, the highest performing SOFC compares favorably with that of other SOFCs containing similar electrolyte and electrode materials [43–46] despite that the electrochemical performance is affected by many factors such as relative thicknesses and composition of each electrode's functional layer, surface area of particles and grain boundaries, dynamic fuel compositions, and relative pressure of fuel delivery. The second set of I-V polarization curves for each SOFC represented a complete thermal cycle after the first evaluation, at different temperatures in a range from 650 to 800 °C and with different concentrations of H_2 in the fuel. These polarization curves are shown in Figs. S5–S7 available in the Supplemental Materials on the ASME Digital Collection. As seen in the polarization curves, the performance drops as the temperature is reduced suggesting that ionic conductivity of the electrolyte and/or the associated activation polarization losses dominate the net polarization losses. Nonetheless, the trend of improving performance with increasing vol% porosity in the anodes remains consistent when temperature is constant. The maximum power density for each I-V evaluation is shown in Figs. S5–S7 which is available in the Supplemental Materials on the ASME Digital Collection and is summarized in Table S3, also available in the Supplemental Materials on the ASME Digital Collection.

The results above show the electrochemical performance increases as porosity is increased in the anode support. This trend suggests that the porosity should be further increased; however, a practical limit exists with respect to the amount of porosity that can be designed into the support of a SOFC which can be defined by determining a minimum practical mechanical strength of the support. Although there is no standard for tubular SOFCs, the mechanical strength of the support should be strong enough so that the cell does not suffer any cracks or factures through all processing methods, necessary evaluations, and eventually during assembly into a SOFC stack.

The MOR is a mechanical figure-of-merit that can be used to help identify a practical mechanical strength. The MOR for the tubes made in this study was determined by a three-point method within a universal testing machine represented by the schematic shown in Fig. 8(*a*). The MOR was determined by measuring the force, *F* (N), at the initial breaking point of the tube shown in Eq. (2) [47,48]

$$\sigma = \frac{FLR}{\pi(R^4 - r^4)} \tag{2}$$

where σ is the MOR (Pa), *L* (m) is the span length between to the two points supporting the sample, *R* (m) is the outer radius of the tube, and *r* (m) is the inner radius. Figure 8(*b*) shows the MOR of anode supports, converted to MPa, after sintering at 1480 °C and in their reduced state with and without the AFL coatings. The

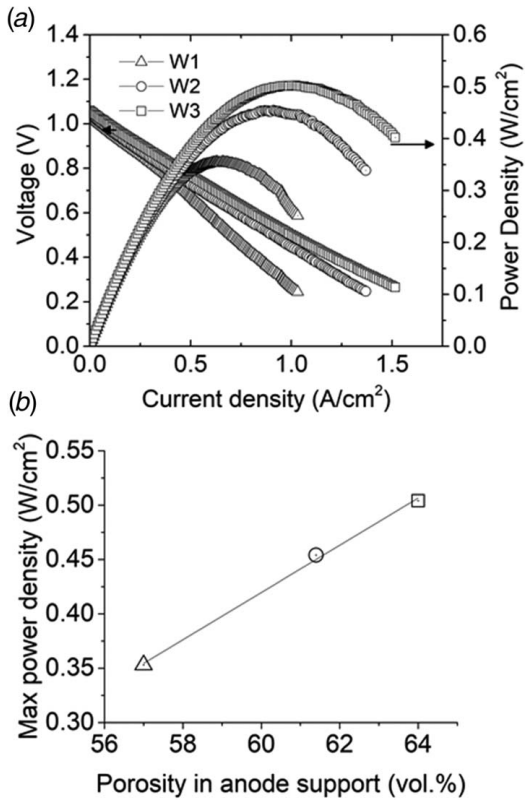

Fig. 7 (*a*) Single-cell power generation from three different cells representing different amounts of porosity in the anode support at 800 °C and with 30% H_2 in the anode fuel and (*b*) maximum power density shown as a function of porosity in the anode support

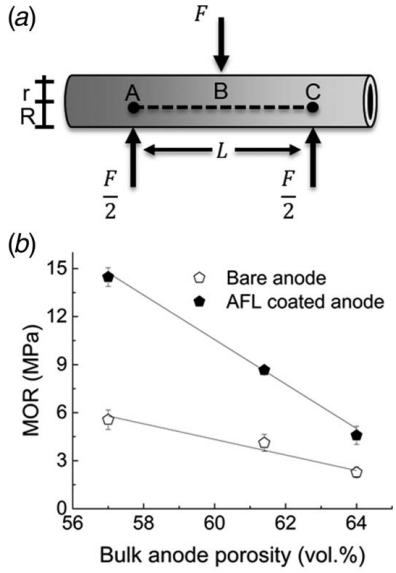

Fig. 8 (*a*) Three-point method for measuring the MOR of a ceramic tubular structure and (*b*) MORs of bare anode supports and anode supports with an AFL with respect to the porosity in the anode support

average maximum MOR values for the three samples in this study with the AFL coating were 14.5, 8.6, and 4.6 MPa having 57.0, 61.4, and 64.0 vol% porosity in the anode support, respectively.

The first observation is the significantly higher MOR for all anode supports with the AFL coatings suggesting that the mechanical strength is dominated by the AFL rather than the anode support itself. The second observation is the decrease in the MOR as the porosity is increased. This is somewhat intuitive as the mechanical strength is expected to decrease as the porosity is increased. And third, the highest MOR average representing the lowest amount of porosity in the anode, *W1,* and with the AFL coating, is much smaller than MOR values observed in other works using different methods of fabrication that show values as high as ~175 MPa when a method referred to as gel-casting is used to make the anode support [48], ~180 MPa for tubes made by an extrusion and consisting of a Sc stabilized zirconia electrolyte supported tube [47], and ~350 MPa for thicker, more conventional anode-supported extruded tubes [49]. Despite that there is no standard mechanical strength for SOFC tubes and therefore understanding the importance of mechanical strength is still unclear, the tubes made in this study have significantly less mechanical strength. If deteremined necessary, future studies could look to increase the mechanical strength of the freeze-casted tubular SOFC without jeopardizing its electrochemical performance. Possible methods include using partially stabilized zirconia, nano-alumina, alumina titanate, or even reducing the average particle size of the materials that make-up the anode support; all of which should increase the mechanical strength without jeopardizing electrochemical performance [50–52].

4 Conclusions

In this work, a freeze-casting method was used to fabricate tubular SOFC anode supports with radially aligned pore channels and with a range of porosity from 57.0 to 64.0 vol% by controlling the solids to water ratio in the casting slurries. Conventional SOFC materials such as Ni-ScYSZ, ScYSZ, and LSM-ScYSZ were used to make the anode, electrolyte, and cathode, respectively, so that overall performance could be compared with previous works. The permeability of the anode support, measured using Darcy's law, was found to be dominated by the AFL, which sits between the anode support and the electrolyte of the SOFC. As porosity was increased from 57 to 64 vol%, the total cell resistance decreased by 35% enabling an increase in electrochemical performance by 42% from 0.35 to 0.50 W/cm^2 when evaluated with 30 vol% H_2 as the fuel at 800 °C. Mechanical characterization showed a practical upper limit of porosity for anode support design with the standard materials. The improved performance by controlling porosity and deeper understanding of the correlation between porosity and concentration polarization losses may shed light on the further optimizations of SOFCs.

Acknowledgment

B. E. and Y. Y. acknowledge the funding support from Texas Center for Superconductivity Center at the University of Houston (TcSUH). We thank Mr. Mingie Shen and Professor Megan Robertson for the help on mechanical measurements.

References

[1] Wachsman, E. D., and Lee, K. T., 2011, "Lowering the Temperature of Solid Oxide Fuel Cells," Science, **334**(6058), pp. 935–939.
[2] Hauth, M., Seidl, M., Postl, A., Sallai, C., Soukup, N., Albert, J., Weinlander, C., Rieberer, R., and Hochenauer, C., 2017, "Development of a Highly Flexible SOFC CCHP System Towards Demand-Oriented Power Generation From Renewable Fuels," *Solid Oxide Fuel Cells 15*, Vol. 78, S. C. Singhal, and T. Kawada, eds., Electrochemical Soc Inc., Pennington, pp. 155–170.
[3] McPhail, S. J., and Bruno Conti, J. K., 2017, *The Yellow Pages of SOFC Technology International Status of SOFC Deployment 2017*, VTT Technical Research Centre of Finland Ltd., Finland, Vol. 32, p. 47.
[4] Krist, K., Gleason, K. J., and Wright, J. D., 1999, *SOFC-Based Residential Cogeneration Systems*, Electrochemical Society Inc., Pennington, Vol. 99, pp. 107–115.
[5] Huang, W. H., Finnerty, C., Sharp, R., Wang, K., and Balili, B., 2017, "High-Performance 3D Printed Microtubular Solid Oxide Fuel Cells," Adv. Mater. Technol., **2**(4), p. 5.
[6] Lawlor, V., Griesser, S., Buchinger, G., Olabi, A. G., Cordiner, S., and Meissner, D., 2009, "Review of the Micro-Tubular Solid Oxide Fuel Cell Part I. Stack Design Issues and Research Activities," J. Power Sources, **193**(2), pp. 387–399.
[7] Mehran, M. T., Park, S. W., Kim, J., Hong, J. E., Lee, S. B., Park, S. J., Song, R. H., Shim, J. H., and Lim, T. H., 2019, "Performance Characteristics of a Robust and Compact Propane-Fueled 150 W-Class SOFC Power-Generation System," Int. J. Hydrogen Energy, **44**(12), pp. 6160–6171.
[8] Sammes, N. M., Du, Y., and Bove, R., 2005, "Design and Fabrication of a 100 W Anode Supported Micro-Tubular SOFC Stack," J. Power Sources, **145**(2), pp. 428–434.
[9] Iwai, H., Shikazono, N., Matsui, T., Teshima, H., Kishimoto, M., Kishida, R., Hayashi, D., Matsuzaki, K., Kanno, D., Saito, M., Muroyama, H., Eguchi, K., Kasagi, N., and Yoshida, H., 2010, "Quantification of SOFC Anode Microstructure Based on Dual Beam FIB-SEM Technique," J. Power Sources, **195**(4), pp. 955–961.
[10] Izzo, J. R., Joshi, A. S., Grew, K. N., Chiu, W. K. S., Tkachuk, A., Wang, S. H., and Yun, W. B., 2008, "Nondestructive Reconstruction and Analysis of SOFC Anodes Using X-Ray Computed Tomography at Sub-50 nm Resolution," J. Electrochem. Soc., **155**(5), pp. B504–B508.
[11] Lu, X. K., Li, T., Bertei, A., Cho, J. I. S., Heenan, T. M. M., Rabuni, M. F., Li, K., Brett, D. J. L., and Shearing, P. R., 2018, "The Application of Hierarchical Structures in Energy Devices: New Insights Into the Design of Solid Oxide Fuel Cells With Enhanced Mass Transport," Energy Environ. Sci., **11**(9), pp. 2390–2403.
[12] Shri Prakash, B., Senthil Kumar, S., and Aruna, S. T., 2014, "Properties and Development of Ni/YSZ as an Anode Material in Solid Oxide Fuel Cell: A Review," Renew. Sust. Energ. Rev., **36**, pp. 149–179.
[13] Fergus, J. W., 2006, "Electrolytes for Solid Oxide Fuel Cells," J. Power Sources, **162**(1), pp. 30–40.
[14] Haslam, J. J., Pham, A. Q., Chung, B. W., DiCarlo, J. F., and Glass, R. S., 2005, "Effects of the Use of Pore Formers on Performance of an Anode Supported Solid Oxide Fuel Cell," J. Am. Ceram. Soc., **88**(3), pp. 513–518.
[15] Luo, L. H., Hou, B. X., Wu, Y. F., Wang, C. C., Cheng, L., Shi, J. J., and Liao, H. M., 2011, "Effect of Graphite Contents on the Electrochemical Performance of SOFC Prepared by Tape Casting," Rare Metal Mat. Eng., **40**, pp. 306–309.
[16] Sarikaya, A., Petrovsky, V., and Dogan, F., 2013, "Development of the Anode Pore Structure and its Effects on the Performance of Solid Oxide Fuel Cells," Int. J. Hydrogen Energy, **38**(24), pp. 10081–10091.
[17] Sumi, H., Yamaguchi, T., Hamamoto, K., Suzuki, T., Fujishiro, Y., and Menon, M., 2013, "Effects of Anode Microstructure on Mechanical and Electrochemical Properties for Anode-Supported Microtubular Solid Oxide Fuel Cells," J. Am. Ceram. Soc., **96**(11), pp. 3584–3588.
[18] Suzuki, T., Hasan, Z., Funahashi, Y., Yamaguchi, T., Fujishiro, Y., and Awano, M., 2009, "Impact of Anode Microstructure on Solid Oxide Fuel Cells," Science, **325**(5942), pp. 852–855.
[19] Jamil, S. M., Othman, M. H. D., Rahman, M. A., Jaafar, J., Ismail, A. F., and Li, K., 2015, "Recent Fabrication Techniques for Micro-Tubular Solid Oxide Fuel Cell Support: A Review," J. Eur. Ceram. Soc., **35**(1), pp. 1–22.
[20] Chen, Y., Bunch, J., Li, T. S., Mao, Z. P., and Chen, F. L., 2012, "Novel Functionally Graded Acicular Electrode for Solid Oxide Cells Fabricated by the Freeze-Tape-Casting Process," J. Power Sources, **213**, pp. 93–99.
[21] Koh, Y. H., Sun, J. J., and Kim, H. E., 2007, "Freeze Casting of Porous Ni-YSZ Cermets," Mater. Lett., **61**(6), pp. 1283–1287.
[22] Lichtner, A. Z., Jauffres, D., Martin, C. L., Bordia, R. K., and Kim, H.-E., 2013, "Processing of Hierarchical and Anisotropic Porosity LSM-YSZ Composites," J. Am. Ceram. Soc., **96**(9), pp. 2745–2753.
[23] Lichtner, A. Z., Jauffres, D., Roussel, D., Charlot, F., Martin, C. L., and Bordia, R. K., 2015, "Dispersion, Connectivity and Tortuosity of Hierarchical Porosity Composite SOFC Cathodes Prepared by Freeze-Casting," J. Eur. Ceram. Soc., **35**(2), pp. 585–595.
[24] Miller, S., Xiao, X. H., Setlock, J., Farmer, S., and Faber, K., 2018, "Freeze-Cast Yttria-Stabilized Zirconia Pore Networks: Effects of Alcohol Additives," Int. J. Appl. Ceram. Technol., **15**(2), pp. 296–306.
[25] Soltani, N., Martinez-Bautista, R., Bahrami, A., Arcos, L., Cassir, M., and Chávez Carvayar, J., 2018, "Fabrication of Aligned Porous $LaNi_{0.6}Fe_{0.4}O_3$ Perovskite by Water Based Freeze Casting," Chem. Phys. Lett., **700**, pp. 138–144.
[26] Moon, J. W., Hwang, H. J., Awano, M., and Maeda, K., 2003, "Preparation of NiO-YSZ Tubular Support With Radially Aligned Pore Channels," Mater. Lett., **57**(8), pp. 1428–1434.
[27] Du, Y., Persky, J., Zhao, K., Ilkhani, H., Woodson, T., Emley, B., and Hedayat, N., 2017, "Fabrication and Electrochemical Characterization of Freeze-Cast Tubular Solid Oxide Fuel Cells," *Solid Oxide Fuel Cells 15*, 78, S. C. Singhal, and T. Kawada, eds., Electrochemical Soc Inc., Pennington, pp. 1885–1895.
[28] Panthi, D., Hedayat, N., Woodson, T., Emley, B. J., and Du, Y., 2019, "Tubular Solid Oxide Fuel Cells Fabricated by a Novel Freeze Casting Method," J. Am. Ceram. Soc., **103**(2), pp. 878–888.
[29] Lankin, M., Du, Y., and Finnerty, C., 2011, "A Review of the Implications of Silica in Solid Oxide Fuel Cells," ASME J. Fuel Cell Sci. Technol., **8**(5), p. 7.

[30] Cable, T. L., and Sofie, S. W., 2007, "A Symmetrical, Planar SOFC Design for NASN's High Specific Power Density Requirements," J. Power Sources, **174**(1), pp. 221–227.
[31] Sofie, S. W., 2007, "Fabrication of Functionally Graded and Aligned Porosity in Thin Ceramic Substrates With the Novel Freeze-Tape-Casting Process," J. Am. Ceram. Soc., **90**(7), pp. 2024–2031.
[32] Seub, J., Leloup, J., Richaud, S., Deville, S., Guizard, C., and Stevenson, A. J., 2017, "Fabrication of Ice-Templated Tubes by Rotational Freezing: Microstructure, Strength, and Permeability," J. Eur. Ceram. Soc., **37**(6), pp. 2423–2429.
[33] Gaudillere, C., and Serra, J. M., 2016, "Freeze-Casting: Fabrication of Highly Porous and Hierarchical Ceramic Supports for Energy Applications," Bol. Soc. Esp. Ceram. Vidr., **55**(2), pp. 45–54.
[34] Liu, R. P., Xu, T. T., and Wang, C. A., 2016, "A Review of Fabrication Strategies and Applications of Porous Ceramics Prepared by Freeze-Casting Method," Ceram. Int., **42**(2), pp. 2907–2925.
[35] Kupecki, J., Kluczowski, R., Papurello, D., Lanzini, A., Kawalec, M., Krauz, M., and Santarelli, M., 2019, "Characterization of a Circular 80%mm Anode Supported Solid Oxide Fuel Cell (AS-SOFC) With Anode Support Produced Using High-Pressure Injection Molding (HPIM)," Int. J. Hydrogen Energy, **44**(35), pp. 19405–19411.
[36] Mukhopadhyay, M., Mukhopadhyay, J., and Basu, R. N., 2013, "Functional Anode Materials for Solid Oxide Fuel Cell—A Review," Trans. Indian Ceram. Soc., **72**(3), pp. 145–168.
[37] Yan, Z., He, A., Hara, S., and Shikazono, N., 2019, "Modeling of Solid Oxide Fuel Cell (SOFC) Electrodes From Fabrication to Operation: Correlations Between Microstructures and Electrochemical Performances," Energy Conv. Manag., **190**, pp. 1–13.
[38] Chen, X. W., and Hong, L., 2010, "An In Situ Approach to Create Porous Ceramic Membrane: Polymerization of Acrylamide in a Confined Environment," J. Am. Ceram. Soc., **93**(1), pp. 96–103.
[39] Tjaden, B., Lane, J., Withers, P. J., Bradley, R. S., Brett, D. J. L., and Shearing, P. R., 2016, "The Application of 3D Imaging Techniques, Simulation and Diffusion Experiments to Explore Transport Properties in Porous Oxygen Transport Membrane Support Materials," Solid State Ion., **288**, pp. 315–321.
[40] Barfod, R., Mogensen, M., Klemenso, T., Hagen, A., Liu, Y.-L., and Vang Hendriksen, P., 2007, "Detailed Characterization of Anode-Supported SOFCs by Impedance Spectroscopy," J. Electrochem. Soc., **154**(4), pp. B371–B378.
[41] Metzger, P., Friedrich, K., Muller-Steinhagen, H., and Schiller, G., 2006, "SOFC Characteristics Along the Flow Path," Solid State Ion., **177**(19–25), pp. 2045–2051.
[42] Shimada, H., Suzuki, T., Yamaguchi, T., Sumi, H., Hamamoto, K., and Fujishiro, Y., 2016, "Challenge for Lowering Concentration Polarization in Solid Oxide Fuel Cells," J. Power Sources, **302**, pp. 53–60.
[43] Liu, R., Cai, G., Li, J., Zhao, C., Wang, S., Wen, T., and Wen, Z., 2010, "Scandia-Stabilized Zirconia-Impregnated (La, Sr)MnO_3 Cathode for Tubular Solid Oxide Fuel Cells," J. Solid State Electrochem., **14**(10), pp. 1923–1928.
[44] Panthi, D., Choi, B., and Tsutsumi, A., 2015, "Fabrication and Evaluation of a Micro-Tubular Solid Oxide Fuel Cell With an Inert Support Using Scandia-Stabilized Zirconia Electrolyte," J. Electrochem. Soc., **162**(14), pp. F1555–F1560.
[45] Sholklapper, T. Z., Radmilovic, V., Jacobson, C. P., Visco, S. J., and De Jonghe, L. C., 2006, "Synthesis and Stability of a Nanoparticle-Infiltrated Solid Oxide Fuel Cell Electrode," Electrochem. Solid St., **10**(4), pp. B74.
[46] Yuan, C., Ye, X., Chen, Y., Chen, T., Liu, M., Li, J., Zhan, Z., and Wang, S., 2014, "Fabrication of Composite Cathode by a New Process for Anode-Supported Tubular Solid Oxide Fuel Cells," Electrochim. Acta, **149**, pp. 212–217.
[47] Hsieh, W.-S., Lin, P., and Wang, S.-F., 2013, "Fabrication of Electrolyte Supported Micro-Tubular SOFCs Using Extrusion and Dip-Coating," Int. J. Hydrogen Energy, **38**(6), pp. 2859–2867.
[48] Morales, M., and Laguna-Bercero, M. A., 2017, "Microtubular Solid Oxide Fuel Cells Fabricated by Gel-Casting: The Role of Supporting Microstructure on the Mechanical Properties," RSC Adv., **7**(29), pp. 17620–17628.
[49] Du, Y., and Sammes, N. M., 2004, "Fabrication and Properties of Anode-Supported Tubular Solid Oxide Fuel Cells," J. Power Sources, **136**(1), pp. 66–71.
[50] Mehran, M. T., Khan, M. Z., Lim, T. H., Lee, S. B., and Song, R. H., 2018, "Effect of Nano-Al_2O_3 Addition on Mechanical Durability of Nickel-Yttria Stabilized Zirconia Anode Support of Solid Oxide Fuel Cells," Ceram. Int., **44**(12), pp. 14824–14833.
[51] Driscoll, D. R., Tokmakian, B. W., Johnson, N. P., Hunt, C. D., and Sofie, S. W., 2017, "Catalyst Enhancing Aluminum Titanate for Increasing Strength of Nickel-Zirconia Cermets," Mater. Lett., **209**, pp. 307–310.
[52] Wang, Y., Walter, M. E., Sabolsky, K., and Seabaugh, M. M., 2006, "Effects of Powder Sizes and Reduction Parameters on the Strength of Ni-YSZ Anodes," Solid State Ion., **177**(17–18), pp. 1517–1527.